

NUMERICAL STUDY OF TURBULENT SUBMERGED BIFURCATED JETS IMPINGEMENT AND INTERACTIONS WITH A FREE SURFACE

B. W. Righolt, S. Kenjereš, R. Kalter, M. J. Tummers and C. R. Kleijn

Section of Transport Phenomena, Department of Chemical Engineering, Faculty of Applied Sciences
Delft University of Technology
and J. M. Burgerscentre for Fluid Dynamics
Julianalaan, 2628 BL Delft
b.w.righolt@tudelft.nl, s.kenjeres@tudelft.nl, c.r.kleijn@tudelft.nl

ABSTRACT

This paper presents the results of the numerical simulation of turbulent submerged jets, issuing from a bifurcated nozzle into a thin cavity with a free surface. The jet Reynolds number is $Re_{jet} = 1.25 \times 10^4$. The jets impinge on solid walls, creating large recirculation zones, moving anti-symmetrically in the symmetric domain. The flow below the free surface causes a significant disturbance of the free surface by the turbulent jets. The free surface is modeled using the Volume of Fluid (VOF) approach, and the turbulence closure is obtained using the standard $k - \epsilon$ T-RANS model as well as with the dynamic Smagorinsky LES model.

The numerical results were assessed with experimental results (Kalter *et al.*, 2013). We have shown that the numerical models capture the physics correctly. The occurrence of a long term asymmetric oscillation is also found in the numerical model for an LES grid of sufficient resolution. However, the inability of the numerical model to predict the close approach of the top recirculation zone to the nozzle is the major source for the differences found between models and experiment. While the dominant oscillation frequency of the long term oscillation was found at approximately $0.09Hz$ in the experiment, the LES model predicts this frequency at $0.14Hz$.

INTRODUCTION

In this paper we will discuss the flow behavior in an open-top cavity with a bifurcated submerged nozzle. This setup is schematically depicted in figure 1. The wide variety of complex flow phenomena makes this an interesting case for numerical simulation. These phenomena include a turbulent channel flow, fast turning flow in the nozzle, a bounded turbulent jet impinging on the wall, large recirculation cells and the interaction of the flow with the free surface.

This setup is derived from the continuous steel casting application. Although simplified, many of the flow features found in the present setup, have also been found in industrial scale casters. The results presented here are therefore of direct relevance for steel producing companies.

For this system it has experimentally been observed that two different flow regimes exist (Kalter *et al.*, 2013). The regimes are clearly apparent at the free surface. In the first regime, gravity waves occur, with a wavelength in the

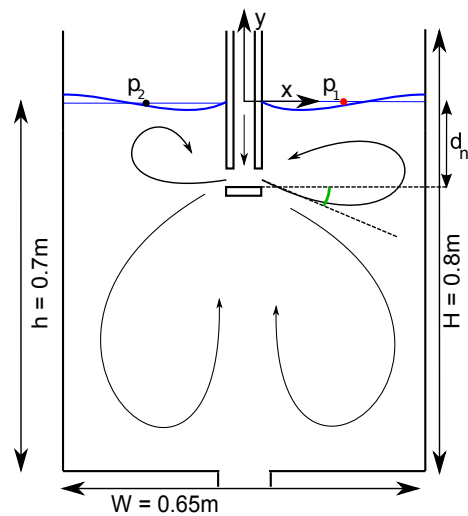


Figure 1. The schematics of the setup considered in this paper is depicted. The rectangular cavity has a thickness of $0.035m$. The inlet nozzle and pipe are square with dimensions of $0.01m$ and wall thickness $0.005m$, while the nozzle depth $d_n = 0.125m$. The points denoted by p_1 and p_2 are monitoring points, and the green line in the jet on the right side indicates the definition of the jet angle, which is negative for a downward directed jet.

order of the width of the cavity (frequency around $1Hz$). In the second regime, the interaction between both jets causes a strong and low frequency oscillation ($f \approx 0.1Hz$). This latter oscillation is anti-symmetric, such that the free surface oscillations on either side are out of phase. It was concluded that the three dimensionality of the flow, possibly flowing between the nozzle and the front and back wall, is crucial for the occurrence of this slow oscillation.

In this paper we will address the results from numerical simulations of the subsurface flow behavior and the interaction with the free surface for a Reynolds number based on the inlet jets of $Re = 1.25 \times 10^4$. The turbulence is modeled using the Transient-Reynolds Averaged Navier-Stokes (T-RANS) standard $k - \epsilon$ model and Large Eddy Simulations (LES) with a dynamic Smagorinsky subgrid scale closure. The mean and transient properties of the flow and the free surface will be assessed against measurement data.

NUMERICAL MODEL

Free surface flow

The free surface flow is modeled using the Volume Of Fluid (VOF) method with a continuum surface force for the surface tension and a compression velocity to keep the interface sharp (Hirt & Nichols, 1981; Brackbill *et al.*, 1992; Rusche, 2002; Weller, 2008; Berberović *et al.*, 2009)

The Navier-Stokes equations for incompressible liquids

$$\frac{\partial \rho v_i}{\partial t} + v_j \frac{\partial \rho v_i}{\partial x_j} = \frac{\partial}{\partial x_j} \left[\mu_{eff} \left(\frac{\partial v_i}{\partial x_j} + \frac{\partial v_j}{\partial x_i} \right) \right] - \frac{\partial p}{\partial x_i} + f_i + \gamma \kappa \frac{\partial \alpha}{\partial x_i}, \quad (1)$$

has been solved. Here α is the indicator function, f_i the body force (gravity), ρ the phase averaged density, μ_{eff} the effective viscosity and κ the curvature of the interface in the Continuum Surface Force (CSF) approach (Brackbill *et al.*, 1992)

The indicator function is 1 in the liquid phase and 0 in the gas phase and indicates the location of the free surface. The transport equation for the indicator function reads

$$\frac{\partial \alpha}{\partial t} + \frac{\partial}{\partial x_j} (\alpha v_j) + \frac{\partial}{\partial x_j} (v_{r,j} \alpha (1 - \alpha)) = 0, \quad (2)$$

where v_r is the compression or relative velocity (Berberović *et al.*, 2009), defined as $v_r = v_l - v_g$. In practice, this is translated into a limiter function blending upwind and central differencing based on the value of α . It should be noted that the VOF method requires significantly smaller time-steps than single phase flow simulations.

Transient-RANS

For the transient Reynolds Average Navier-Stokes simulations, we used the standard $k - \epsilon$ model with wall functions (Kenjereš & Hanjalić, 2009). The Navier-Stokes equations 1 are solved for the mean velocity, with the effective viscosity $\mu_{eff}/\rho = \nu + \nu_t = \nu + C_\mu \frac{k^2}{\epsilon}$, where the separate equations for the turbulent kinetic energy k and turbulent dissipation rate ϵ are solved. A non-uniform hexahedral mesh consisting of 10^6 control volumes will be used, where time integration is evaluated using a second order implicit scheme and the convective terms are discretized using the minmod flux limiter.

Large Eddy Simulation

The subgrid scale closure used in the LES simulations, is the dynamic Smagorinsky model as proposed by Lilly (1992). Lilly (1992) argued that calculating the dynamic coefficient on local grid points can lead to computational instability and suggests averaging to avoid excessively large values. The approach as outlined by Zang *et al.* (1993) was employed, which comes down to area weighted averaging over the face-interpolated values, which for perfectly hexahedral control volumes is $\langle f \rangle = \frac{1}{2} f + \frac{1}{12} \sum_{nb=1}^6 f_{nb}$. The dynamic Smagorinsky coefficient is then determined from $C = \frac{1}{2} \frac{\langle L_{ij} M_{ij} \rangle}{\langle M_{ij}^2 \rangle}$. The subgrid scale viscosity is now modeled as $\nu_t = (C\Delta)^2 \mathcal{S}$, with Δ the grid size and \mathcal{S} the characteristic rate of strain.

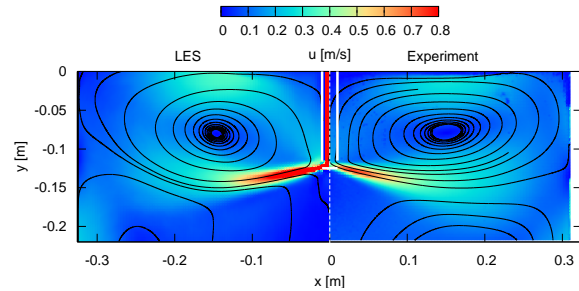


Figure 2. The contours of the velocity magnitude and stream traces for the LES simulation (left) and in the experimental results (right). The equilibrium position of the interface is located at $y = 0$.

For the numerical simulation, the equations are discretized on an uniform mesh consisting of approximately 10^7 control volumes. Time is integrated with a second order implicit scheme, while the convective and diffusive terms are discretized using a central differencing scheme.

RESULTS

This section describes results from the numerical simulations, which are assessed using experimental measurement data (Kalter *et al.*, 2013). The Reynolds number based on the jet entrance into the cavity is $Re_{jet} = 12,500$ and the two fluids are water and air. First we will focus on the flow underneath the free surface, then we will focus on the interplay of the sub-surface flow with the free surface and pinpoint the challenges remaining.

Subsurface flow

Figure 2 shows the mean velocity field for both the LES simulation and the experiment. The experimental data was obtained from PIV measurements, aimed at resolving the flow outside the jet region. It is observed that the recirculation zone as found in the experiment is well predicted. It is noted that the mean recirculation cell seems slightly more elongated in the experiment. Figure 3 shows the horizontal velocity component along several vertical lines across the domain. The main differences in the mean velocity profiles are found near the free surface, where the $k - \epsilon$ model predicts significantly higher velocities.

The dynamics of the system appears in the transient behavior of the recirculation cell. Therefore, the center of the recirculation cell on one side of the domain is tracked in time. The center of the recirculation zone is determined from the maximum of the function $\Gamma_1(\vec{x})$ proposed by Graftieux *et al.* (2001):

$$\Gamma_1(\vec{x}) = \frac{1}{N} \sum_{i=1}^N \frac{|(\vec{x} - \vec{x}_i) \times \vec{u}(\vec{x}_i)|}{|(\vec{x} - \vec{x}_i)| |\vec{u}(\vec{x}_i)|}. \quad (3)$$

Here \vec{x} is the position vector and \vec{x}_i the position vector of N surrounding locations in the neighbourhood of \vec{x} . \vec{u} is the two-component velocity vector.

In figure 4 time traces of the center of the recirculation zone are shown for both the experimental and the numerical results for a period of 40s. It shows how the recirculation cell moves back and forth between the wall and the nozzle.

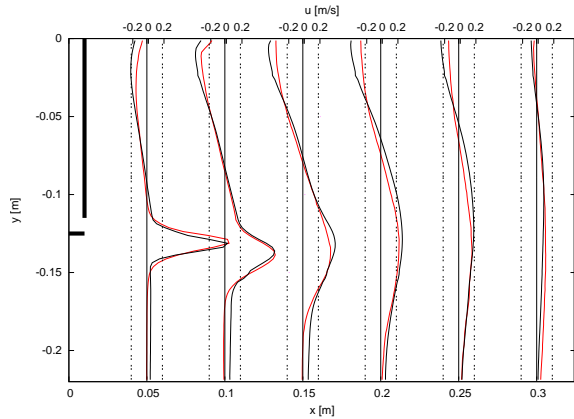


Figure 3. The horizontal velocity component along vertical lines in the domain for the numerical simulations, i.e. T-RANS standard $k - \epsilon$ (—, black) closure and LES with dynamic Smagorinsky sub-grid modeling (—, red).

This behavior is clearly observed in both experiment and simulation.

Comparison of the time trace of the recirculation cell center in the experiment with both the $k - \epsilon$ and LES model shows that the position furthest away from the nozzle is reached at the same position for the experiment and numerical simulations, namely at $x = 0.21m$. However, in the experiment, the recirculation zone moves closer to the nozzle ($0.06m$) than in the numerical approaches ($0.09m$).

Figure 5 shows the horizontal position of the recirculation cell center in time. The center of the recirculation cell undergoes a periodic movement in the top of the system. It can be seen from this figure, that the steepest slopes upward or downward, are the same in experiment and simulation. This means that the velocity of the recirculation cell center across the domain is well predicted. In the experiment, the recirculation cell approaches the nozzle much closer, and thus travels a longer path. Combining this, it follows that the oscillation frequency observed in the numerical simulation and in the experiment are not in agreement. From figure 5 it is calculated that the long term oscillation period for the experiment (10s) is substantially longer than for both models (8s for $k - \epsilon$, 7s for dynamic Smagorinsky).

It was experimentally observed that the recirculation cell oscillates in an anti-symmetric way on opposite sides of the system, even though the set-up is symmetric. This was also observed in the LES simulation, as can be seen in figure 6, which shows three snapshots of the flow field during half a period of the long term oscillation. Initially the recirculation zone on the right side is located far away from the nozzle, while the recirculation zone on the left is close to the nozzle, while half a period later the situation is reversed.

The angle with which the jet issues from the nozzle is shown in figure 7. The jet angle is defined in figure 1, where a negative angle refers to a downward direction jet. In relation to figure 5 it is seen that the frequency of oscillation of the recirculation zone is in agreement with the jet angle oscillation frequency. When the jet is negative (downward jet), the recirculation cell center is located close to the side wall and when the jet angle increases, the recirculation cell will move towards the nozzle. Kalter *et al.* (2013) showed that an upward directed jet induces a high pressure gradient between recirculation cell center and free surface,

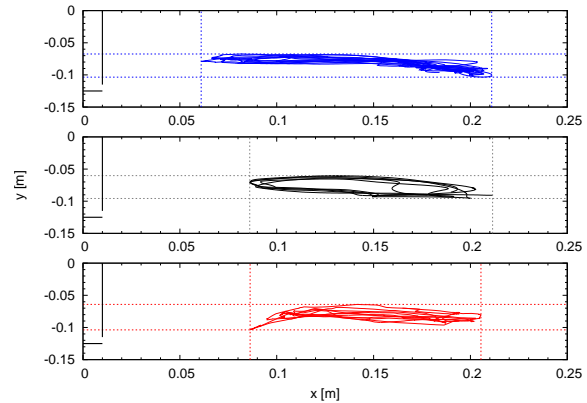


Figure 4. Time traces of the position of the recirculation cell center for the experiment (top, —, blue), the standard $k - \epsilon$ model, (middle, —, black) and the dynamic Smagorinsky model (bottom, —, red). The dashed lines indicate the outermost vertical and horizontal position of the recirculation cell center.

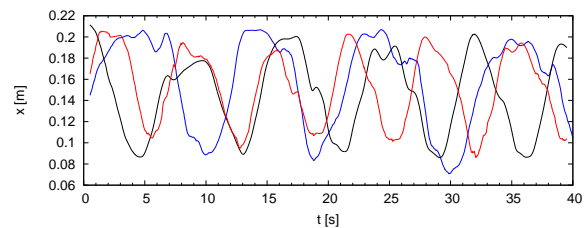


Figure 5. The horizontal position in time of the center of the recirculation zone is depicted for the experiment (—, blue), standard $k - \epsilon$ T-RANS (—, black) and dynamic Smagorinsky LES (—, red). The position of the recirculation cell center was determined from the Γ_1 function (equation 3).

which rapidly decreases when the recirculation zone collapses by fluid escaping through the gaps between between nozzle and the front and back walls of the cavity.

For LES simulations on a coarser mesh with computational control volumes of double size in every direction (10^6 control volumes), one may conclude from figure 7 (bottom) that the jet frequency on a coarser mesh shows a closer match to the experimentally obtained frequency. However, the jet is directed downwards than in the experiment and is also oscillating less, thus enlarging the recirculation cell. This also increases the interaction time with the opposite recirculation cell and thus reduces the frequency.

In terms of the second order statistics we will focus on the resolved part of the turbulent kinetic energy $k_{res} = \frac{1}{2}(\overline{u'u'} + \overline{v'v'} + \overline{w'w'})$ and the Reynolds stress terms $\overline{u'v'}$, where the primed quantities refer to the fluctuating parts of the velocity components. One should realize, that for the LES simulation, the filtered velocity components are used, while for the T-RANS simulations the turbulent quantities are based on the ensemble averaged velocities. For the T-RANS simulations the modeled part of the terms is added, \bar{k} and $-C_\mu \frac{k^2}{\epsilon} \left(\frac{\partial u}{\partial y} + \frac{\partial v}{\partial x} \right)$ respectively.

Figure 8 shows contours of the turbulent kinetic energy, which is highest in the jet region. Furthermore, there is an increased amount of turbulent kinetic energy in the impingement region, which is highest in the $k - \epsilon$ -model. It is

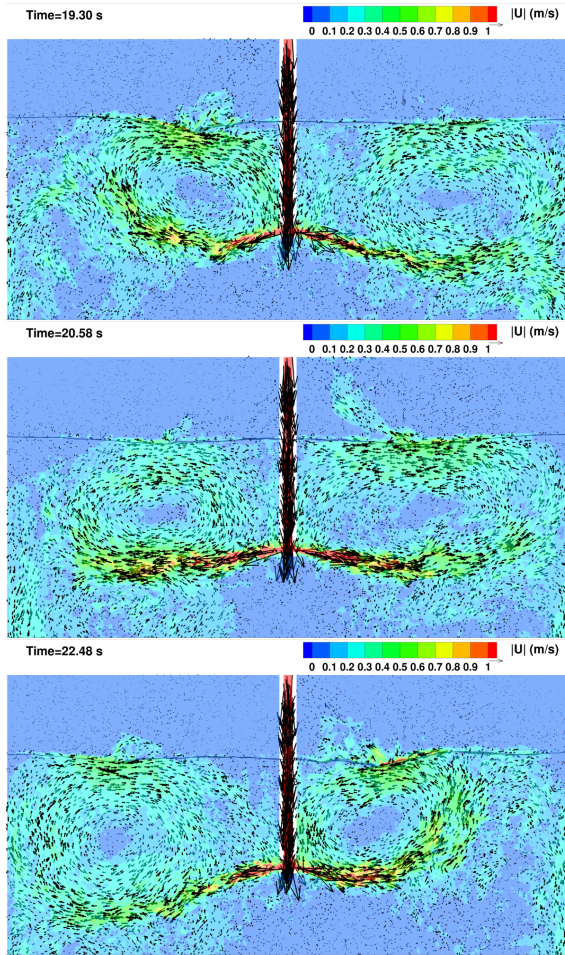


Figure 6. Snapshots of the flow field and the free surface for the LES simulation. The snapshots are taken approximately a quarter of the long oscillation period apart.

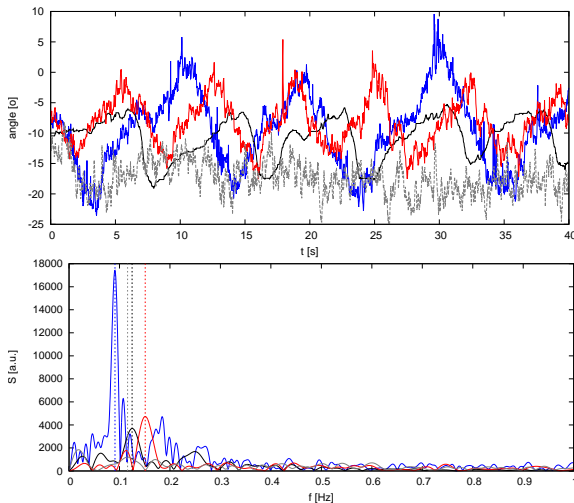


Figure 7. Time series (top) and the related frequency spectra (bottom) for the angle of the jet issuing into the cavity with respect to the horizontal. Depicted for the experiment (—, blue), the $k - \epsilon$ model (—, black), the dynamic Smagorinsky model (—, red) and the dynamic Smagorinsky model on a coarse mesh (—, gray). The maxima in the frequency spectra are amplified with a vertical line.

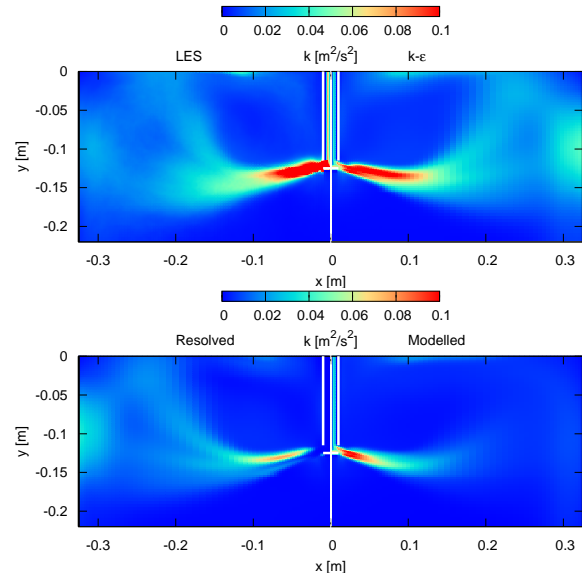


Figure 8. Top: The turbulent kinetic energy k for the LES simulation (left) and $k + \overline{k_{mod}}$ for the $k - \epsilon$ model (right) Bottom: The contribution to the total turbulent kinetic energy of the $k - \epsilon$ -model, k (left) and $\overline{k_{mod}}$ (right).

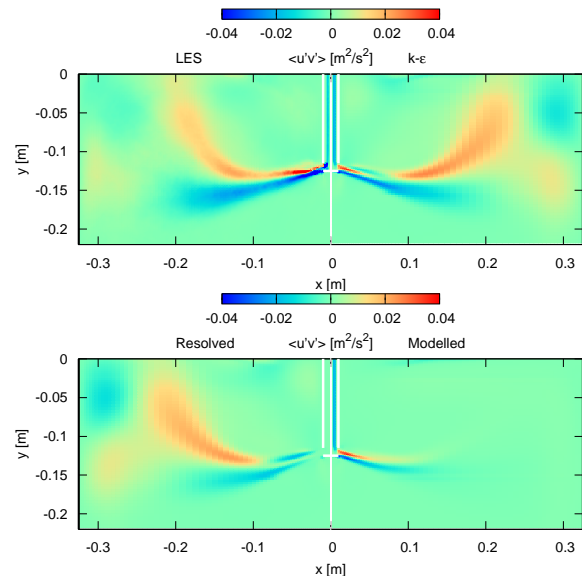


Figure 9. Top: The resolved part of the Reynolds stress $\overline{u'v'}$ for the LES simulation (left) and the total Reynolds stress for the $k - \epsilon$ -model (right). Bottom: The contribution to the total Reynolds stress for the $k - \epsilon$ -model, $\overline{u'v'}$ (left) and $-C_\mu \frac{k^2}{\epsilon} \left(\frac{\partial u}{\partial y} + \frac{\partial v}{\partial x} \right)$ (right).

well-known that the $k - \epsilon$ model overpredicts the turbulent kinetic energy in impingement regions. Following the peak k in the downstream direction, it is seen that the local peak turbulent kinetic energy separates in two branches or lobes, which can be associated with the large-scale oscillation of the recirculation zone.

Figure 9 shows the Reynolds stress component $\overline{u'v'}$. For both the Reynolds stress components as well as the turbulent kinetic energy (figure 8) the modeled part has a substantial contribution only in the region close to the jet.

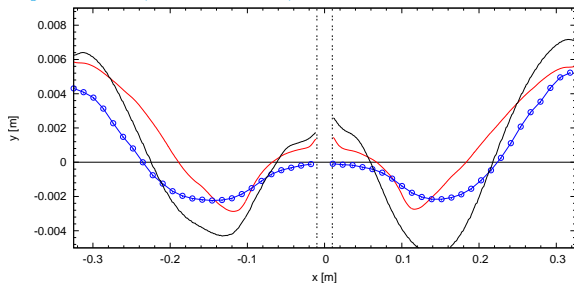


Figure 10. Time averaged free surface elevation for the experiment (\circ , blue), the $k - \epsilon$ -model ($-$, black) and the dynamic Smagorinsky model ($-$, red). The vertical dashed lines indicate the position of the nozzle.

Free surface

The major interest in this paper is the position of the free surface, and how well it can be predicted by the numerical models that are employed.

The position of the free surface is determined from the $\alpha = 0.5$ -iso-surface (equation 2). The time average of this position is depicted in figure 10. The deformation near the outer walls and a minimum in the elevation between the nozzle and the wall are found in both experiment and simulations. The $k - \epsilon$ model overpredicted velocities near the free surface (see figure 3), which results in a larger free surface deformation than the LES model and the experiment. Even though the mean velocities were relatively well predicted by the LES model, the mean surface elevation deviates from the experimental results.

Figure 6 shows snapshots of the flow, clearly demonstrating the movement of the recirculation zone, but also that the minimum in the free surface is right above the center of the recirculation cell. When the recirculation zone is at the outermost position, a clear local minimum does not appear. At the location of the local minimum, the velocities just below the surface are relatively high, which can result in the inclusion of bubbles Kalter *et al.* (2013), which is challenging for a VOF simulation.

The anti-symmetric behavior of the flow in this system is also clearly apparent at the free surface as can be seen from figure 11. Figure 11 shows the free surface elevation as a function of time for two monitoring points at opposite sides of the nozzle. The experimentally observed behavior is found with both numerical models and is a result of the interplay between the recirculation cells at opposite sides of the nozzle.

In figure 12 the free surface elevation is depicted as a function of space and time. Black regions are related to the minimum in the free surface elevation. For the numerical simulations it was observed that this minimum is related to the position where the liquid in the top of the recirculation zone submerges (see also figure 6). From figure 12, it can be argued that this minimum in the free surface elevation approaches the nozzle ($x = 0$) closer in the experiment than in the simulations, which is related to the recirculation zone center getting closer to the nozzle in the experiments.

Figure 13 shows the frequency spectra calculated from the time series in figure 11. It is seen that the spectrum for the experiment shows three dominant peaks, while the spectra for the numerical simulation methods show two. Furthermore, it is observed that the peak with the lowest frequency can be related to the long term anti-symmetric oscillation, and this frequency was also apparent in the oscillation.

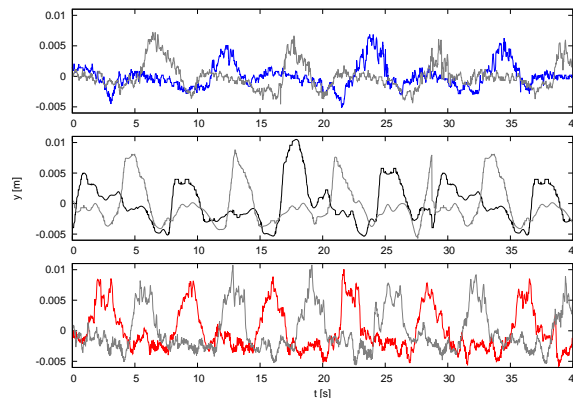


Figure 11. This figure shows the time series of the elevation of two monitoring points lying at the free surface (see figure 1) at $x = \pm 0.175$ for the experiment (top, $-$, blue), the standard $k - \epsilon$ model, (middle, $-$, black) and the dynamic Smagorinsky model (bottom, $-$, red), where the gray line is referring to the left-most monitoring point in all figures.

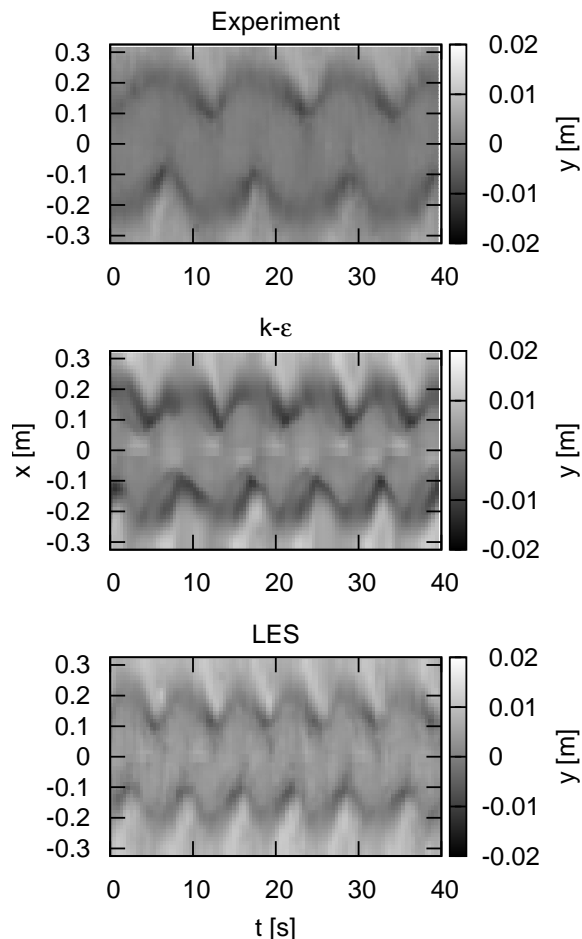


Figure 12. The above contours show the elevation of the free surface in time and space. Light regions indicate peak elevation and dark regions indicate valleys, for the experiment (top), $k - \epsilon$ (middle) and the dynamic Smagorinsky model (bottom).

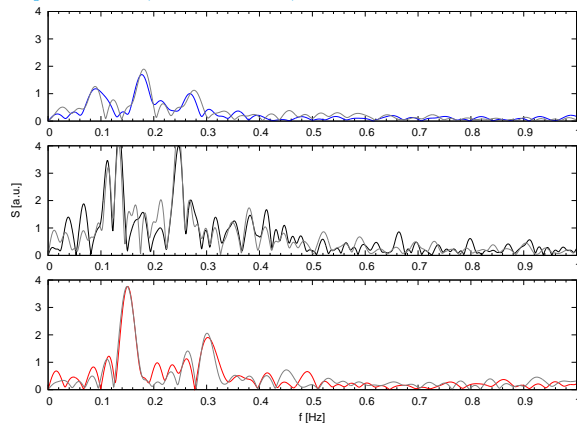


Figure 13. This figure shows the frequency spectrum of the elevation of two monitoring points lying at the free surface, at $x = \pm 0.175$ for the experiment (top, —, blue), the standard $k - \varepsilon$ model, (middle, —, black) and the dynamic Smagorinsky model (bottom, —, red), where the gray line is referring to the left-most monitoring point in all figures. This frequency spectrum is derived from the time series as depicted in figure 11.

lation of the jet (see figure 7). In all cases, a secondary peak with double frequency is found.

CONCLUSION

We have numerically studied the flow from a submerged bifurcated nozzle in a thin cavity and the influence of the flow on the free surface deformation, using the standard $k - \varepsilon$ T-RANS closure model and the dynamic Smagorinsky LES sub-grid scale model.

The numerical results have been assessed using experimental data. Qualitatively, the numerical simulations model the physics of the flow correct. Long-term anti-symmetric oscillations of the recirculation zones in the top of the cavity, that were earlier found in experiment (Kalter *et al.*, 2013), have also been found in the numerical simulation. The main difference between the results from the experiment and numerical models is the frequency in the long term anti-symmetric oscillation of the recirculation cells in both sides of the cavity. The long-term oscillation frequency for the simulations ($0.12 - 0.14\text{Hz}$) is significantly higher than in the frequency found in the experiment (0.09Hz). The origin of the difference in frequency was found in the temporal position of the recirculation cell in the top of the cavity, which is moving closer to the nozzle in the experiment than in the numerical simulations.

While the mean velocity was predicted relatively well, and the mean elevation of the free surface qualitatively shows the same features as in the experiment, it was found that the mean free surface elevation profiles are not predicted accurately by both numerical models. In the $k - \varepsilon$

model the predicted mean free surface elevation is substantially larger than in the experiment. In the LES model, the order of magnitude of minimum and maximum free surface deformation were well predicted, however, the position of the minimum was not correctly predicted. This is also related to the position of the recirculation zone moving less close to the nozzle. The lowest oscillation frequency of the free surface was found to match the oscillation frequency of the jet issuing from the nozzle into the cavity. However, also higher harmonics of this frequency were found at the free surface in both the experiment and in the numerical simulations.

We thus have shown that the numerical models captures the physics correctly. The occurrence of a long term asymmetric oscillation is included by the model for an LES grid of sufficient resolution. However, the inability of the numerical model to include the close approach of the top recirculation zone to the nozzle, is the major source for the differences found between the numerical models and the experimental results.

REFERENCES

- Berberović, E., van Hinsberg, N. P., Jakirlić, S., Roisman, I. V. & Tropea, C. 2009 Drop impact onto a liquid layer of finite thickness: Dynamics of the cavity evolution. *Physical Review E* **79** (3), 036306.
- Brackbill, J. U., Kothe, D. B. & Zemach, C. 1992 A continuum method for modeling surface tension. *Journal of Computational Physics* **100** (2), 335–354.
- Graftieaux, L., Michard, M. & Grosjean, N. 2001 Combining PIV, POD and vortex identification algorithms for the study of unsteady turbulent swirling flows. *Measurement Science and Technology* **12** (9), 1422.
- Hirt, C. W. & Nichols, B. D. 1981 Volume of fluid (VOF) method for the dynamics of free boundaries. *Journal of Computational Physics* **39** (1), 201–225.
- Kalter, R., Tummers, M. J., Kenjereš, S. & Kleijn, C. R. 2013 Oscillations of the fluid flow and the free surface in a cavity with a submerged bifurcated nozzle. *International Journal of Heat and Fluid Flow* (submitted).
- Kenjereš, S. & Hanjalić, K. 2009 Tackling complex turbulent flows with transient RANS. *Fluid Dynamics Research* **41**, 012201.
- Lilly, D. K. 1992 A proposed modification of the germano subgrid-scale closure method. *Physics of Fluids A: Fluid Dynamics* **4** (3), 633.
- Rusche, H. 2002 Computational fluid dynamics of dispersed two-phase flows at high phase fractions. PhD thesis, Imperial College.
- Weller, H. G. 2008 A New Approach to VOF-based Interface Capturing Methods for Incompressible and Compressible Flow. *Tech. Rep.*. OpenCFD.
- Zang, Y., Street, R. L. & Koseff, J. R. 1993 A dynamic mixed subgrid scale model and its application to turbulent recirculating flows. *Physics of Fluids A: Fluid Dynamics* **5** (12), 3186–3196.